The Astrophysical Journal Letters, 815:L16 (6pp), 2015 December 10 doi:10.1088/2041-8205/815/1/L16

PROPAGATING DISTURBANCES IN THE SOLAR CORONA AND SPICULAR CONNECTION

Tanmoy Samanta[1], Vaibhav Pant[1], and Dipankar Banerjee[1,2]
[1] Indian Institute of Astrophysics, Koramangala, Bangalore 560034, India; tsamanta@iiap.res.in
[2] Center of Excellence in Space Sciences, IISER Kolkata, India
Received 2015 September 8; accepted 2015 November 23; published 2015 December 9

ABSTRACT

Spicules are small, hairy-like structures seen at the solar limb, mainly at chromospheric and transition region lines. They generally live for 3–10 minutes. We study these spicules in a south polar region of the Sun with coordinated observations using the *Interface Region Imaging Spectrograph* (*IRIS*) and the Atmospheric Imaging Assembly (AIA) instruments on board the *Solar Dynamics Observatory*. Propagating disturbances (PDs) are observed everywhere in the polar off-limb regions of the Sun at coronal heights. From these simultaneous observations, we show that the spicules and the PDs may have originated through a common process. From spacetime maps, we find that the start of the trajectory of PDs is almost cotemporal with the time of the rise of the spicular envelope as seen by *IRIS* slit-jaw images at 2796 and 1400 Å. During the return of spicular material, brightenings are seen in AIA 171 and 193 Å images. The quasi-periodic nature of the spicular activity, as revealed by the *IRIS* spectral image sequences, and its relation to coronal PDs, as recorded by the coronal AIA channels, suggest that they share a common origin. We propose that reconnection-like processes generate the spicules and waves simultaneously. The waves escape while the cool spicular material falls back.

Key words: Sun: corona – Sun: magnetic fields – Sun: oscillations – Sun: transition region – Sun: UV radiation

Supporting material: animations

1. INTRODUCTION

White light and Extreme Ultra Violet (EUV) emission from the polar region of the solar corona shows distinct, bright, ray-like structures known as polar plumes (van de Hulst 1950; Saito 1958, 1965; Deforest et al. 1997; DeForest & Gurman 1998). Quasi-periodic propagating intensity perturbations are frequently observed in the polar plumes and inter-plume regions with periods ranging from 5 to 30 minutes. The measured speed of these propagating disturbances (PDs) is around 150 km s^{-1}. These outward PDs are generally interpreted as slow magnetoacoustic waves propagating through the plumes and inter-plumes region because their speeds are similar to the sound speed (DeForest & Gurman 1998; Ofman et al. 1999, 2000; Banerjee et al. 2000, 2009, 2011; O'Shea et al. 2007; Krishna Prasad et al. 2011; Gupta et al. 2012; Gupta 2014; Su 2014; Banerjee & Krishna Prasad 2015).

Using EUV observations from the *Solar TErrestrial RElations Observatory*, McIntosh et al. (2010) studied high speed jets of plasma traveling along the plume structures with a mean velocity around 135 km s^{-1}. Those jets were quasi-periodic with periodicities of 5–25 minutes. Tian et al. (2011c) also showed that high-speed repetitive outflows, which originate near magnetic network elements both in the quiet-Sun and coronal holes (CHs), propagate along plume structures with an average speed of ∼120 km s^{-1}. McIntosh et al. (2010) suggested that the PDs are nothing but these jets originating from the upper chromosphere, which propagate to higher corona and contribute to the solar wind. They further conjectured that these jets will supply adequate energy to the fast solar wind. Pucci et al. (2014) found radially moving radiance variations both in the plume and inter-plume regions. Comparing the apparent outflow speeds at different temperature passbands they concluded that the observed radiance variations represent the material outflows.

The quasi-periodic intensity enhancement, the Doppler shift, and the line width enhancements in coronal structures have also recently been interpreted as due to high-speed upflows from spectroscopic observations in magnetic regions of the solar atmosphere (De Pontieu et al. 2009, 2011; De Pontieu & McIntosh 2010; Martínez-Sykora et al. 2011; Tian et al. 2011a, 2011b; Tian et al. 2012). Pant et al. (2015) have studied an on-disk plume as seen by the Atmospheric Imaging Assembly (AIA) and their connection to transition region jets seen in *IRIS*. They found that small-scale chromospheric jet-like features are linked with the generation of PDs within the plume. De Pontieu et al. (2011) found that spicules seen in AIA 304 Å channels propagate upward and fall back following parabolic paths, whereas, at the same time, they also found that enhanced emissions seen in 171 Å propagate upward into the corona with speeds of ∼100 km s^{-1}. It has yet to be explored whether similar behavior can been seen in the off-limb corona and thus this is the subject of the present analysis.

Recently, Jiao et al. (2015) claimed that the spicular activities in the solar transition region, as seen in the AIA 304 Å passband, are responsible for the generation of the PDs in the polar regions of the corona as observed in the AIA 171 Å images. However, the exact connection between spicule and PDs, as well as the nature of the PDs, still remains a mystery. Furthermore, for the solar wind studies, it is important to have a better understanding of the nature of these PDs and their origin. To find out the spicular connection to the coronal PDs, we use simultaneous *IRIS* data along with coronal data from AIA.

2. DATA ANALYSIS AND RESULTS

2.1. Observation and Data Reduction

The data was obtained from coordinated observations using the *Interface Region Imaging Spectrograph* (*IRIS*) satellite (De Pontieu et al. 2014) and the AIA instruments (Lemen et al. 2012) on board the *Solar Dynamics Observatory*

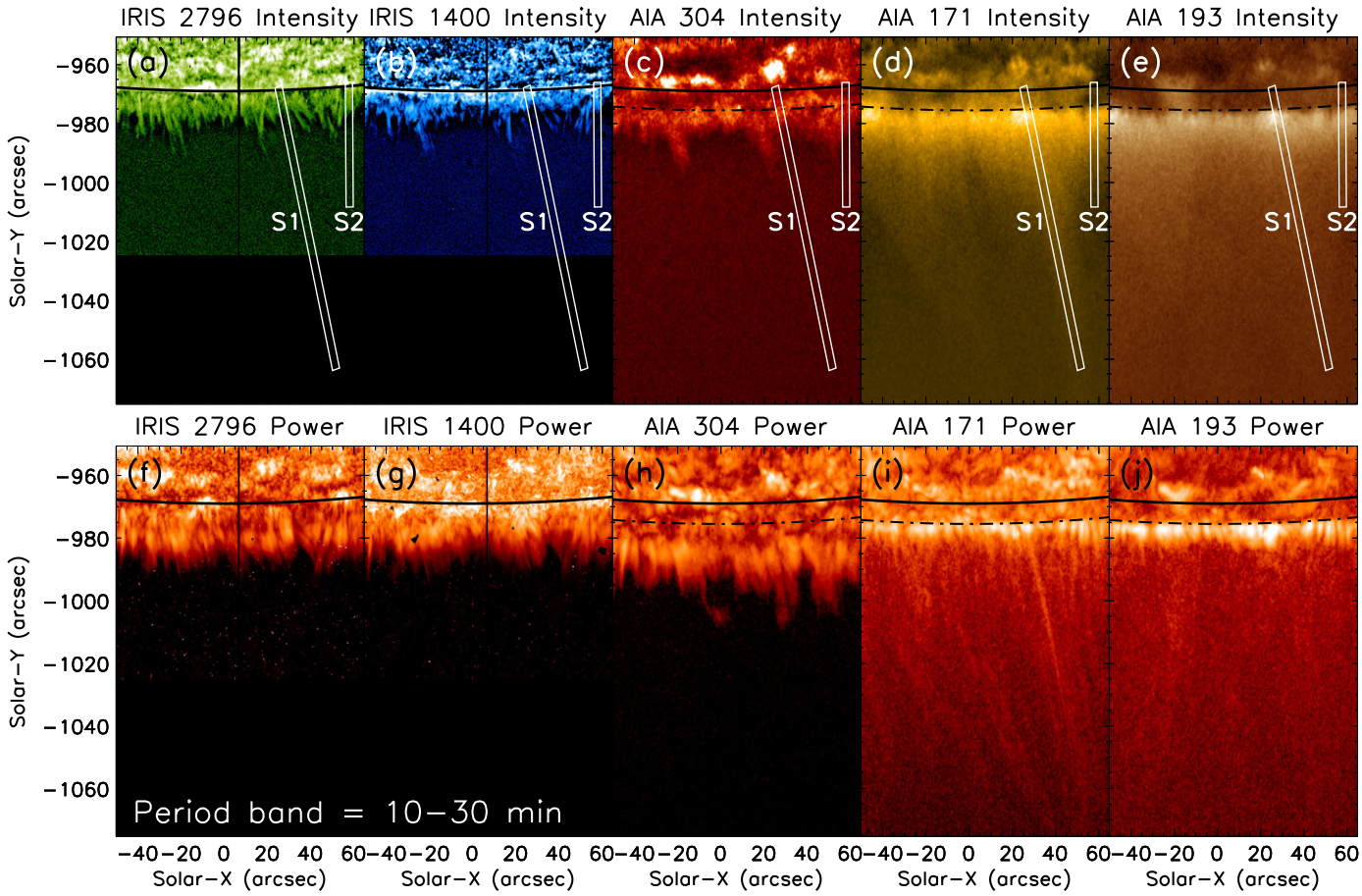

Figure 1. (a)–(e) Display a portion of the south polar region of the Sun as seen in different filtergram images taken from *IRIS* and *SDO*/AIA instruments on 2014 February 21 as marked. The vertical black line on each *IRIS* SJIs represents the position of the *IRIS* slit. The solid black curve line on each image shows the location of the solar limb. The dotted–dashed black line on each AIA image displays the location of the solar limb as identified from the AIA 171 Å image. The field of view (FOV) of *IRIS* is smaller than the selected window of AIA images, which makes it appear dark in SJIs where *IRIS* FOV does not overlap with AIA. Two boxes (S1 and S2) show the location of the selected slits used to construct the spacetime (*X*–*T*) plot (see Figures 2 and 3). (f)–(j) Show the distribution of power (power maps) of corresponding top panel channels. The power maps are constructed by taking the average power of the 10–30 minute period band.

(An animation of this figure is available.)

(*SDO*). Observations were performed from 11:25 UT to 12:55 UT on 2014 February 21. Slit-jaw images (SJIs) from *IRIS* filtergrams centered at 2796 and 1400 Å and dominated by Mg II and Si IV emission lines, respectively, were analyzed. AIA filtergram images centered at 304, 171, and 193 Å and dominated by He II, Fe IX, and Fe XII emission, respectively, were also selected for the analysis. The *IRIS* 2796 Å passband is sensitive to emission from plasma at temperatures of ∼10,000–15,000 K and *IRIS* 1400 Å is sensitive to temperatures of ∼ 60,000–80,000 K. The AIA 304, AIA 171, and AIA 193 Å filters' response functions peak at 0.05, 0.8, and 1.25 MK respectively.

IRIS observed the south pole of the Sun in sit-and-stare mode. We used *IRIS* Level 2 processed data, which is corrected for dark-current, flat-field, and geometrical corrections etc. All of the *IRIS* SJIs were taken with an 8 s exposure time and a cadence of 19 s. The pixel size of SJIs and AIA are 0.″166 and 0.″6 respectively. The AIA images were taken with a 12 s cadence. The pixel size of AIA is interpolated to match with *IRIS* for easier comparison. All of the AIA channels were coaligned and derotated to compensate for solar rotation. The *IRIS* SJIs and AIA images were coaligned using *IRIS* 1400 Å and AIA 1600 Å images (as described in Skogsrud et al. 2015).

Figures 1(a)–(e) show the south polar region of the Sun as seen from *IRIS* and AIA channels. We should point out here that CH was not seen clearly on the south pole during the observation, hence the the region can be characterized as a quiet Sun. Furthermore, distinct extended plume structures were not so clearly visible from the original images. Usually, when there is a underlying deep CH present, plume structures are clearly visible.

2.2. Power Maps

PDs in the corona often repeat with a timescale of 10–30 minutes. To find the global behavior of PDs, we constructed power maps in the period band of 10–30 minutes. We performed a wavelet analysis in the time series at each pixel location to estimate the distribution of power. A background trend is removed by subtracting a 30 minute running average of the original time series to remove periods longer than 30 minutes. Figures 1(f)–(j) show the distribution of power (referred to as power maps) within the 10–30 minute period band of *IRIS* 2796 Å, *IRIS* 1400 Å, AIA 304 Å, AIA

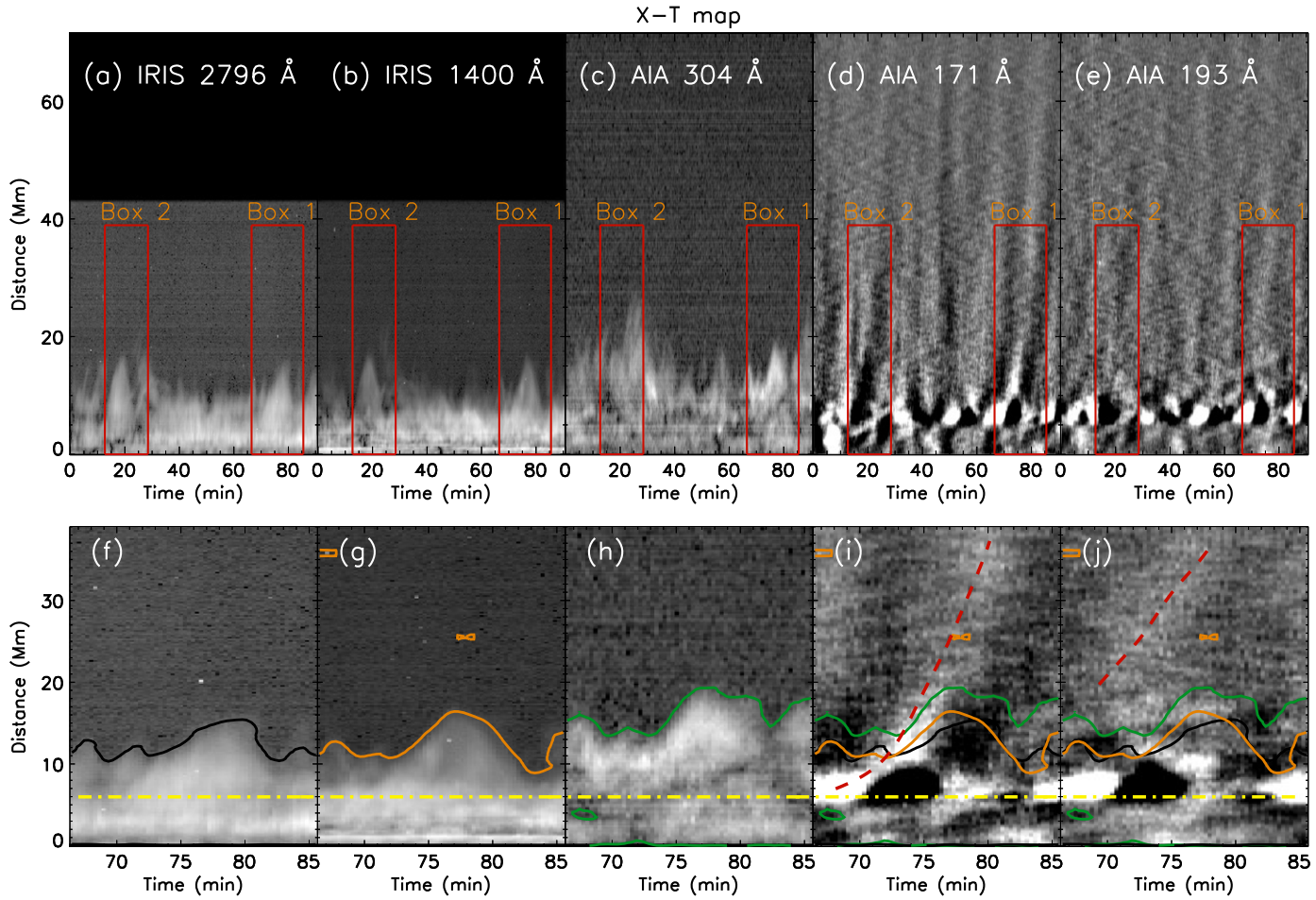

Figure 2. *X–T* plots corresponding to the S1 slit and different passbands as marked. A zoomed view of the region inside the red rectangular Box 1 (marked in the upper panels) is shown in (f)–(j). Black, orange, and green contours show the envelopes of the spicular temporal evolution as seen in the *IRIS* 2796 Å SJI, *IRIS* 1400 Å SJI, and AIA 304 Å channels. These contours are overplotted in the AIA 171 Å and AIA 193 Å *X–T* map for comparison. The dotted–dashed horizontal line in yellow represents the limb of the Sun as seen in AIA 171 and 193 Å. Dashed red curves track the PDs observed in AIA 171 and 193 Å.

(Animations a and b of this figure are available.)

171 Å, and AIA 193 Å channels. The power maps of *IRIS* 2796 Å, *IRIS* 1400 Å, and AIA 304 Å show that the power in this period band is limited to lower heights (within $\sim 20''$ from the solar limb). These channels are sensitive to the chromospheric and transition region temperature, which is dominated by spicular activity and the power is probably limited to lower heights due to this. At some locations, we note that the strong power is seen up to higher heights. In AIA 171 Å and AIA 193 Å power maps, we observed two kinds of features, one reaching to larger distances (see the location of S1 slit) and the other which has comparatively higher power, but is confined to shorter distances (see the location of S2 slit). In the next subsection, we will study in detail the behavior of PDs in these regions (within S1 and S2).

2.3. Spacetime Plot

In this subsection, we focus on the plume-like structure marked by the S1 slit in Figure 1 for a detailed time evolution of PDs. We constructed the *X–T* map to study the temporal evolution of the region inside the S1 slit. The signal in the AIA channels is low for off-disk features, hence, to improve the signal to noise, we have used a thick slit with a width of $3''.32$. The average intensity along the width of the slit was used to construct the *X–T* maps of different channels. The *X–T* map of AIA 171 and 193 Å were processed by removing a smoothed background trend along the time axis to enhance the visibility of the alternating ridges. The results are shown in Figure 2. The *X–T* maps of the *IRIS* 2796 Å, *IRIS* 1400 Å, and AIA 304 Å, which are sensitive to chromospheric and transition region temperatures, show the evolution of several spicules. On the other hand, the dark and bright ridges extended over longer distances are seen in the AIA 171 and 193 Å channels. The zoomed view of a portion of the *X–T* map is shown in the bottom panels of the same figure. The temporal evolution of spicules are seen in *IRIS* 2796 Å, *IRIS* 1400 Å, and AIA 304 Å appears to have sub-structures rising and falling in all passbands. It appears that they roughly follow the parabolic path as seen in many spicules. Contours are over-plotted by choosing some intensity threshold on the *IRIS* 2796 Å, *IRIS* 1400 Å, and AIA 304 Å channels, which are shown by black, orange, and green contours respectively. It covers the envelope of the spicular temporal evolution. These three contours are also overplotted in the AIA 171 and 193 Å *X–T* maps. The trajectories of the PDs are marked by red dashed

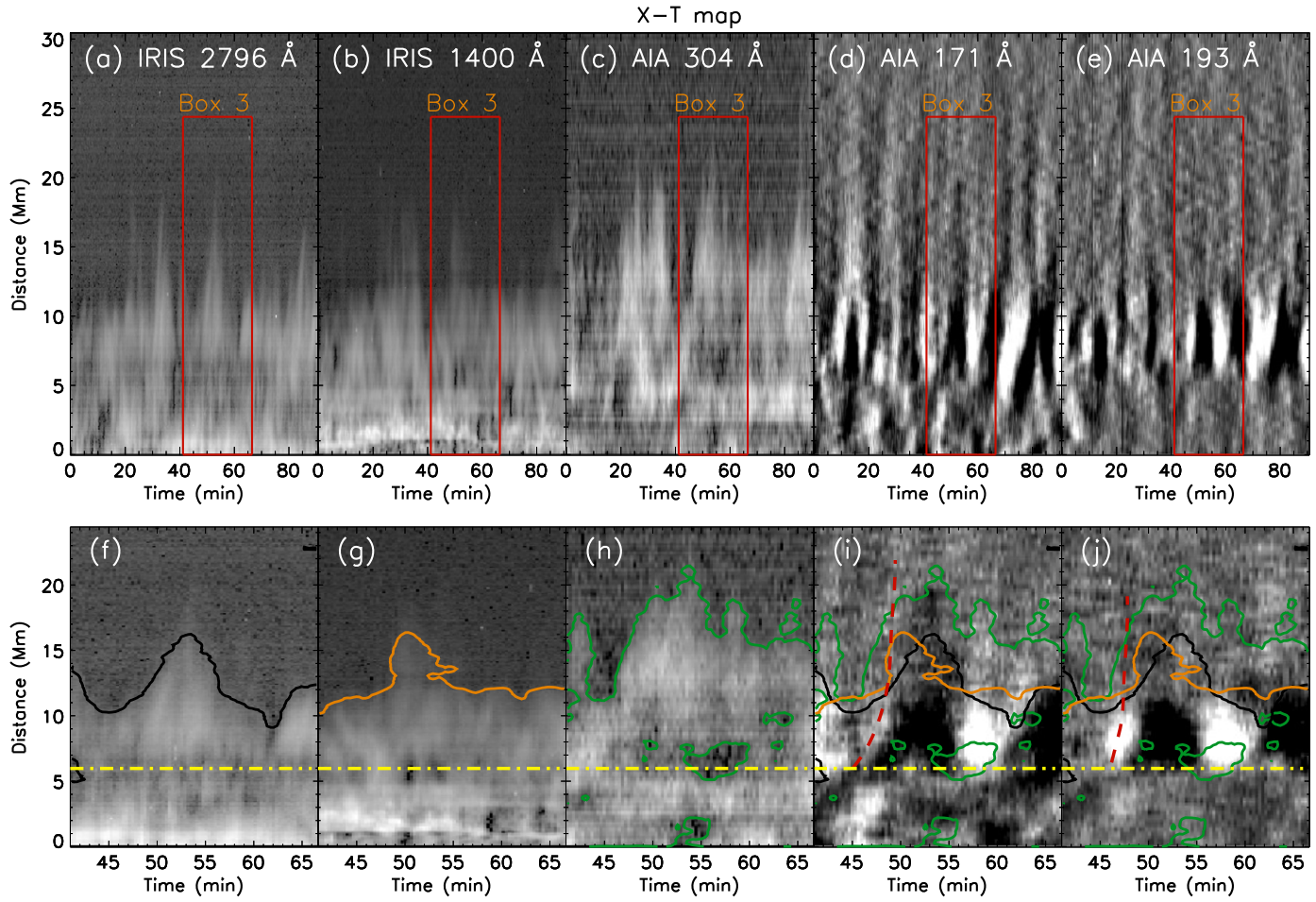

Figure 3. *X–T* plots corresponding to the S2 slit and different passbands as marked. All panels are similar to those in Figure 2.
(An animation of this figure is available.)

curves, as shown in the zoomed AIA 171 and 193 Å panels of Figures 2 and 3.

A similar procedure was adopted for the slit S2 analysis. The slit width of the slit S2 is the same as S1. The *X–T* maps for different channels are shown in Figure 3. In the lower panels of Figures 2 and 3, we note that the start of the trajectory of PDs is almost cotemporal with the time of the rise of the spicular envelope. We also note that the falling of the spicular envelope is followed by brightenings and the generation of another PD in AIA 171 and 193 Å.

It is worth noting that PDs in Figure 2 (following a plume-like structure) are propagating to higher heights (65 Mm), as compared to PDs in Figure 3, which seem to propagate roughly about 30 Mm. Thus, power was confined to lower heights at the slit S2 location.

2.4. Measurements of the Propagating Speed of the PDs

To follow the PDs and its connection with rapidly evolving spicular activities, we produce a composite *X–T* plot (Figure 4). The *IRIS* channels corresponding to the bottom part of the maps (as marked) allow us to identify the spicules and their temporal evolution whereas the AIA channels corresponding to the upper part of the maps allow us to identify the PDs quite clearly. In order to see the alternating ridges clearly, we enhance the contrast by subtracting the smooth background in *X–T* maps. This procedure is followed for AIA channels (i.e., the upper part of the maps in Figure 4). For the *IRIS* channel (the lower part of the maps), no background subtraction is performed because no enhancement in the lower part of *X–T* maps is needed. This further demonstrates that when a spicule is observed by the chromospheric channel of *IRIS*, a PD seems to be generated and/or amplified in the AIA coronal channels. This also confirms that the PDs seem to be quasi-periodic with a periodicity that is governed by the repetition time scale of occurrence of the spicules. From this figure, we also fit the ridges manually using eye estimation and found the range of velocities from 98–148 $\mathrm{km\,s^{-1}}$ in AIA 171 Å and 103–191 $\mathrm{km\,s^{-1}}$ in AIA 193 Å. There is a large uncertainty in the measured speed, thus we cannot confirm if we observe different speeds in the two different channels. We find the speeds of spicules from 22–91 $\mathrm{km\,s^{-1}}$ corresponding to *IRIS* 1400 Å images and 16–57 $\mathrm{km\,s^{-1}}$ for *IRIS* 2796 Å images. Since the speeds are higher than sound speed at chromospheric levels, these spicules could be generated by reconnection at lower heights.

3. CONCLUSION

PDs are ubiquitous in the solar atmosphere and it has recently been suggested by Jiao et al. (2015) that spicules can trigger coronal PDs. From their study, using the AIA data

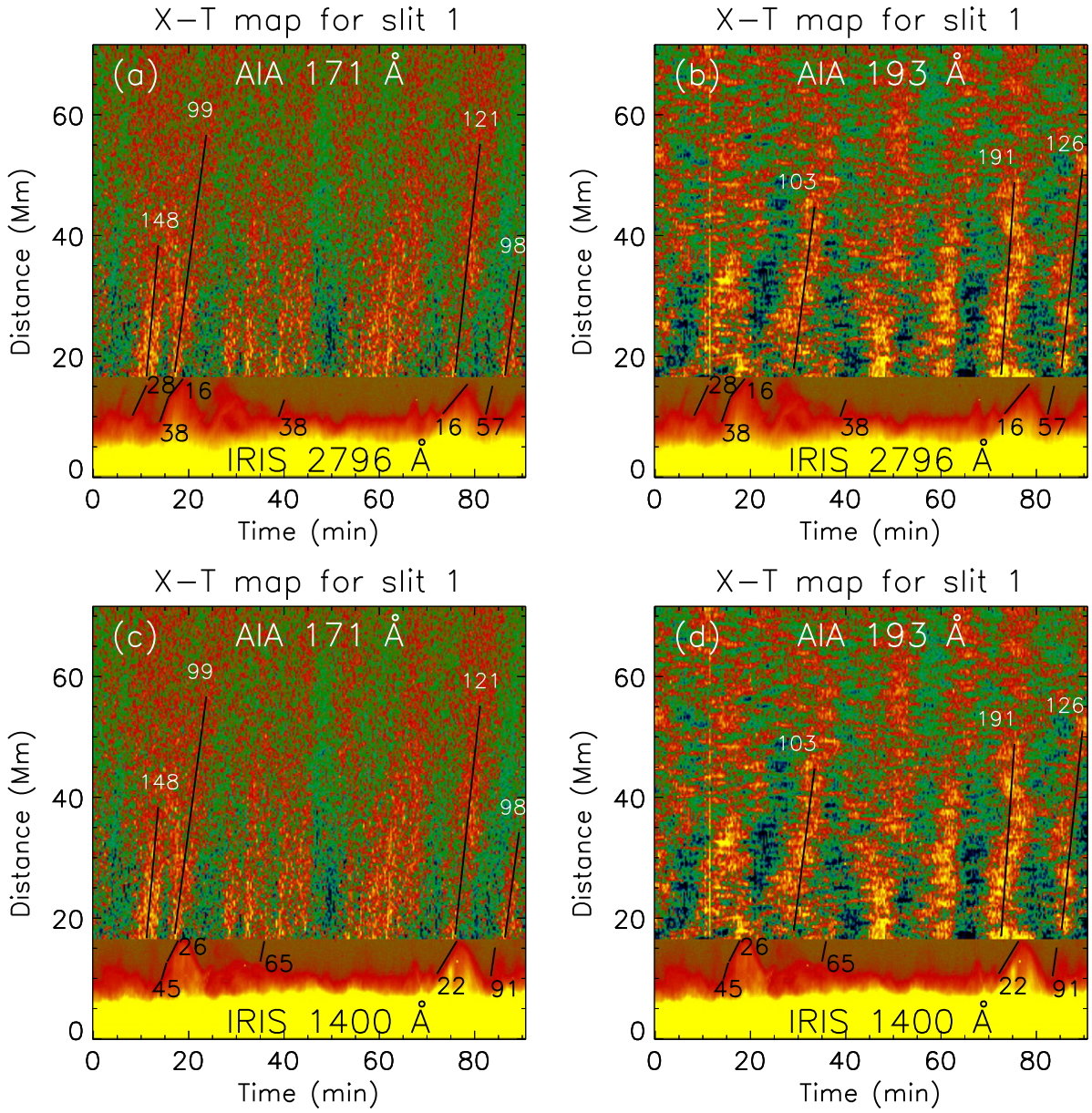

Figure 4. *X–T* corresponding to slit location S1 (along a plume-like structure) showing connection between spicular activities as seen by *IRIS* channels (bottom) and PDs as seen by coronal AIA channels (top). The slanted black lines are used to measure the speeds. Measured speeds in km s^{-1} are printed.

alone, they provided a possible link between spicular activities and the generation of PDs. They used the AIA 304 Å channel to identify the spicules. Though, they did not comment on the nature of the PDs. We extended that work using higher cadence and higher resolution *IRIS* spectral images to study the dynamical behavior of the spicular activity and, while combining AIA channels, we are able to confirm the link with better confidence. We believe that a combination of chromospheric and transition region channels of *IRIS* and transition region and coronal channels of AIA is better suited for this kind of study. We also point out a possible connection between the small-scale, short-lived, cool spicular structures with the very-large-scale, long-lived, hot plume structures. We find that the start of trajectory of PDs is almost cotemporal with the time of the rise of the spicular envelope and the spicular material fall is cotemporal with brightenings followed by the generation of another PD in AIA 171 and 193 Å. The cotemporal generation of spicules and PDs suggests that they might have a common origin. We should point out here that there could be a projection effect and that we cannot rule out the possibility that the spicules and PDs may not be in the same position; however, statistically, we find cotemporal and cospatial matches in most of the cases studied. Figure 4 illustrates the quasi-periodic nature of the spicular activity as revealed by the *IRIS* spectral image sequences and its relation to coronal PDs as recorded by the coronal AIA channels. We propose that reconnection-like processes generate the spicules and waves simultaneously. The waves escape while the cool spicular material falls back. The PDs as seen have a mixed signature of waves and flows at lower heights while at the extended coronal heights the wave signature is dominant. There is also a signature of acceleration of these PDs as represented by the curved, red, dashed lines in the lower panels of Figures 2 and 3. The nature of PDs in our case is not always confirmatory, but the presence of alternating

bright and dark ridges and reaching of accelerating PDs to higher heights in slit position S1 (see Figures 2 and 4) suggest a more wave-like nature while manual fitting of PDs to derive speeds is not accurate enough to confirm wave-like behavior. We should also point out that we did not have any CHs in the polar regions and thus the presence of plume-like structures was also not very clear at all locations. At slit position S2, we find that PDs are not going to higher heights. Thus, power is confined to lower heights close to the limb. The enhancement in power is due to repeated generation of cool spicular material seen as dark features in hot AIA channels. Due to almost straight ridges, poor signal to noise, we could not measure the speeds of these PDs convincingly and thus cannot comment on their nature. It is also possible that at the time of the generation of spicules (due to heating together with reconnection and/or driven by *p*-modes) the hot material can escape following the open magnetic field lines and thus cause intensity enhancements in the AIA 171 and 193 Å channels while spicular material falls back because it is denser and cooler than escaping hot material. With the existing spectral imaging data, the connection of spicules and PDs are subject to line-of-sight uncertainties. For further confirmation and a better understanding of the nature of the PDs, we need simultaneous chromospheric and coronal long spectral time sequences.

We thank the *IRIS* team for proving the data in the public domain. We also thank the referee for valuable comments. *IRIS* is a NASA small explorer mission developed and operated by LMSAL with mission operations executed at the NASA Ames Research center and major contributions to downlink communications funded by the Norwegian Space Center (NSC, Norway) through an ESA PRODEX contract.

REFERENCES

Banerjee, D., Gupta, G. R., & Teriaca, L. 2011, SSRv, 158, 267
Banerjee, D., & Krishna Prasad, S. 2015, arXiv:1505.04475
Banerjee, D., O'Shea, E., & Doyle, J. G. 2000, SoPh, 196, 63
Banerjee, D., Teriaca, L., Gupta, G. R., et al. 2009, A&A, 499, L29
De Pontieu, B., & McIntosh, S. W. 2010, ApJ, 722, 1013
De Pontieu, B., McIntosh, S. W., Hansteen, V. H., & Schrijver, C. J. 2009, ApJL, 701, L1
De Pontieu, B., McIntosh, S. W., Carlsson, M., et al. 2011, Sci, 331, 55
De Pontieu, B., Title, A. M., Lemen, J. R., et al. 2014, SoPh, 289, 2733
DeForest, C. E., & Gurman, J. B. 1998, ApJL, 501, L217
Deforest, C. E., Hoeksema, J. T., Gurman, J. B., et al. 1997, SoPh, 175, 393
Gupta, G. R. 2014, A&A, 568, A96
Gupta, G. R., Teriaca, L., Marsch, E., Solanki, S. K., & Banerjee, D. 2012, A&A, 546, A93
Jiao, F., Xia, L., Li, B., et al. 2015, ApJL, 809, L17
Krishna Prasad, S., Banerjee, D., & Gupta, G. R. 2011, A&A, 528, L4
Lemen, J. R., Title, A. M., Akin, D. J., et al. 2012, SoPh, 275, 17
Martínez-Sykora, J., De Pontieu, B., Hansteen, V., & McIntosh, S. W. 2011, ApJ, 732, 84
McIntosh, S. W., Innes, D. E., de Pontieu, B., & Leamon, R. J. 2010, A&A, 510, L2
Ofman, L., Nakariakov, V. M., & DeForest, C. E. 1999, ApJ, 514, 441
Ofman, L., Nakariakov, V. M., & Sehgal, N. 2000, ApJ, 533, 1071
O'Shea, E., Banerjee, D., & Doyle, J. G. 2007, A&A, 463, 713
Pant, V., Dolla, L., Mazumder, R., et al. 2015, ApJ, 807, 71
Pucci, S., Poletto, G., Sterling, A. C., & Romoli, M. 2014, ApJ, 793, 86
Saito, K. 1958, PASJ, 10, 49
Saito, K. 1965, PASJ, 17, 1
Skogsrud, H., Rouppe van der Voort, L., De Pontieu, B., & Pereira, T. M. D. 2015, ApJ, 806, 170
Su, J. T. 2014, ApJ, 793, 117
Tian, H., McIntosh, S. W., & De Pontieu, B. 2011a, ApJL, 727, L37
Tian, H., McIntosh, S. W., De Pontieu, B., et al. 2011b, ApJ, 738, 18
Tian, H., McIntosh, S. W., Habbal, S. R., & He, J. 2011c, ApJ, 736, 130
Tian, H., McIntosh, S. W., Wang, T., et al. 2012, ApJ, 759, 144
van de Hulst, H. C. 1950, BAN, 11, 150